 doi:10.20944/preprints202011.0176.v1

Article

An ultra-high-Q lithium niobate microresonator integrated with a silicon nitride waveguide in the vertical configuration for evanescent light coupling

Jianhao Zhang [1,2], Rongbo Wu [1,2], Min Wang [3,4,*], Youting Liang [3,4], Junxia Zhou [3,4], Miao Wu[3,4], Zhiwei Fang [3,4], Wei Chu [4,] and Ya Cheng [1,3,4,5,6,7,8,*]

1 State Key Laboratory of High Field Laser Physics, Shanghai Institute of Optics and Fine Mechanics, Chinese Academy of Sciences, Shanghai 201800, China; jhzhang@siom.ac.cn (Jianhao Zhang); rbwu@siom.ac.cn (Rongbo Wu)

2 Center of Materials Science and Optoelectronics Engineering, University of Chinese Academy of Sciences, Beijing 100049, China

3 State Key Laboratory of Precision Spectroscopy, East China Normal University, Shanghai 200241, China; zwfang@phy.ecnu.edu.cn (Zhiwei Fang);15253172638@163.com (Youting Liang); 52180920026@stu.ecnu.edu.cn (Junxia Zhou); wumiao1993@126.com (Miao Wu)

4 The Extreme Optoelectromechanics Laboratory (XXL), School of Physics and Electronic Science, East China Normal University, Shanghai 200241, China; wchu@phy.ecnu.edu.cn (Wei Chu)

5 Collaborative Innovation Center of Extreme Optics, Shanxi University, Taiyuan 030006, China

6 Collaborative Innovation Center of Light Manipulations and Applications, Shandong Normal University, Jinan 250358, China

7 CAS Center for Excellence in Ultra-Intense Laser Science, Shanghai 201800, China

8 Shanghai Research Center for Quantum Sciences, Shanghai 201315, China

* Corresponding author: mwang@phy.ecnu.edu.cn; ya.cheng@siom.ac.cn

Abstract: We demonstrate hybrid integration of a lithium niobate microring resonator with a silicon nitride waveguide in the vertical configuration to achieve efficient light coupling. The microring resonator is fabricated on a lithium niobate on insulator (LNOI) substrate using photolithography assisted chemo-mechanical etching (PLACE). A fused silica cladding layer is deposited on the LNOI ring resonator. The silicon nitride waveguide is further produced on the fused silica cladding layer by first fabricating a trench in the fused silica using focused ion beam (FIB) etching for facilitating the evanescent coupling, followed by formation of the silicon nitride waveguide on the bottom of the trench. The FIB etching ensures the required high positioning accuracy between the waveguide and the ring resonator. We achieve Q-factors as high as 1.4×10^7 with the vertically integrated device.

Keywords: lithium niobate microring resonator; silicon nitride waveguide; photolithography assisted chemo-mechanical etching

1. Introduction

Lithium niobate (LN) has long been recognized as an important material platform for integrated photonic devices because of its wide transparent window, high nonlinear coefficient and excellent electro-optical property [1]. In particular, the latest advancement of the fabrication technologies of high-quality photonic micro- and nanostructures on lithium niobate on insulator (LNOI) have further promoted the development of integrated photonics on the LNOI platform. The building block photonic structures such as microresonator and optical waveguide are typically fabricated on LNOI substrate using either maskless focused ion beam (FIB) milling or lithographic processing involving argon ion milling [2-11]. Meanwhile, a chemo-mechanical etching process (termed photolithography assisted chemo-mechanical etching (PLACE) hereafter) has been developed to achieve ultra-high surface smoothness, resulting in high-quality (high-Q) microdisk resonator with a Q-factor of 4×10^7

Preprints (www.preprints.org) | NOT PEER-REVIEWED | Posted: 4 November 2020 doi:10.20944/preprints202011.0176.v1

and ultra-low-loss optical waveguide with a propagation loss of 0.03 dB/cm [12-14]. So far, a broad range of nonlinear optical processes have been demonstrated with the ultra-high-Q LN microresonators fabricated using the PLACE technology, ranging from optomechanics [15] and optical frequency comb [16] to nonlinear frequency conversion [17] and on-chip micro-disk lasing.

In order to excite the nonlinear optical effects, light must be efficiently coupled into the microresonaotors using either a fiber taper [18] or an integrated optical waveguide [19]. The on-chip integration of the microresonator and the coupling optical waveguide provides an efficient means for up scaling of the photonic integration circuits (PICs) which is critical for some applications such as photonic computation and quantum information processing [20], etc. However, in the PLACE scheme, both the low-loss optical waveguides and high Q microresonators are generated using the chemical-mechanical polishing (CMP) technique. In the CMP process, it is required that the distance between the closely located photonic structures should be on the micrometer scale but not the nanometer scale, otherwise the LNOI in the narrow gap between the neighboring structures cannot be efficiently removed by polishing. In this case, the lateral evanescent coupling between a microresonator and a waveguide is difficult to achieve simply because of the fact that the evanescent coupling in the visible and near infrared ranges requires the gap width to be on the order of a few hundred nanometers. For this reason, on-chip evanescent coupling has not been realized between an optical waveguide and a microresonator fabricated using the PLACE technique.

Here, we overcome the difficulty by utilizing a vertical coupling scheme between a crystalline LN microring resonators and a silicon nitride (SiN) waveguide. SiN is also considered as an attractive candidate for monolithic integration of photonic circuits because of its low propagation loss. Importantly, SiN has a refractive index close to that of LN, making it easy to fulfill the phase matching condition between the SiN waveguide and the LN microresonator. We characterize the integrated device by measuring the Q-factor of the fabricated LN microresonator.

2. Materials and Methods

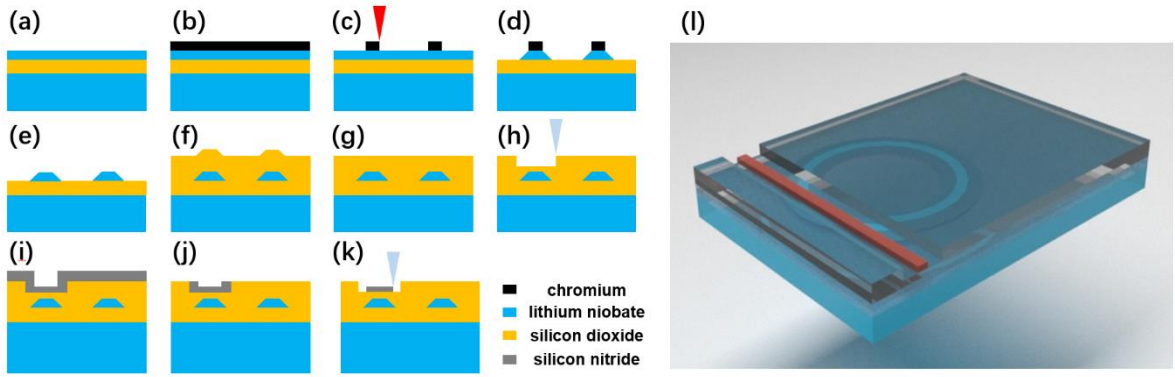

Figure 1. (**a~k**) Process flow of fabricating a lithium niobate (LN) microring resonator coupling with a silicon nitride (SiN) waveguide in the vertical configuration. (**l**) 3D diagram of the coupling structure.

The microring resonator is fabricated on a commercially available x-cut LNOI wafer with a thickness of 900 nm (NANOLN, Jinan Jingzheng Electronics Co., Ltd., Jinan, Shandong, China). The LN thin film is bonded to a 2 μm-thick SiO_2 layer supported by a 500-μm-thick LN substrate. The configuration of the LNOI wafer is illustrated in Fig. 1(a), followed by the schematic of process flow as shown in Fig. 1(b)-(k). In general, the fabrication procedures include: (1) deposition of a thin layer of chromium (Cr) with a thickness of 400 nm on the surface of the LNOI by magnetron sputtering (Fig. 1(b)); (2) space-selective ablation of a Cr layer coated on top of the LNOI to generate the pattern of the microring resonator using a focused femtosecond laser beam (Fig. 1(c)). In this step, the femtosecond laser ablation was conducted by a commercial laser system (Pharos, LightConversion,

Preprints (www.preprints.org) | NOT PEER-REVIEWED | Posted: 4 November 2020 doi:10.20944/preprints202011.0176.v1

Lithuania) at a repetition rate of 500 kHz and a scan speed of 40 mm/s. The center wavelength of the femtosecond laser was 1030 nm, and the pulse width was set to be ~ 270 fs. To obtain a high ablation resolution, a 100× objective lens (M Plan Apo NIR, Mitutoyo, Japan) with a numerical aperture (NA) of 0.7 was employed to pattern the Cr layer. Femtosecond laser ablation was carried out by translating the sample with a 3D motion stage (ABL1500-ANT130, Aerotech Inc., USA). (3) etching of the LNOI layer by CMP (Fig. 1(d)). In this step, the LN without being covered by the Cr mask will be completely removed, while the LN protected by Cr mask will survive from the CMP because of the high hardness of Cr; (4) removal of the residual Cr mask left on the surface of LNOI by chemical wet etching, and further eliminate the roughness by a second CMP process (Fig. 1(e)); (5) deposition of the SiO_2 film on the LNOI waveguide to form the cladding layer by plasma enhanced chemical vapor deposition (PECVD) (Fig. 1(f)); (6) polishing the surface of SiO_2 cladding layer with the third CMP (Fig. 1(g)); (7) patterning of the SiO_2 layer using focused ion beam (FIB) etching (Fig. 1(h)). In particular, the depth of the etched trench can be controlled with an accuracy of ~1nm using the FIB etching; (8) deposition of a SiN film on the SiO_2 layer by PECVD to fill the trench fabricated in the SiO_2 cladding layer (Fig. 1(i)); (9) removing the SiN above the SiO_2 layer with the fourth CMP (Fig. 1(j)); (10) patterning of the SiN film in the trench using FIB etching to form the waveguide (Fig. 1(k)). More details of the femtosecond laser micromachining of Cr, the CMP processing and the FIB etching can be found elsewhere [12,13,14]. A schematic 3D view of the hybrid LN and SiN coupling structure is shown in Fig. 1(l).

3. Results

Figure 2(a) shows the top-view scanning electron micrograph (SEM) of the vertically coupled LN microring and SiN waveguide. The profiles of the microring buried beneath SiO_2 layer can be distinguished in the SEM image. The radius of the LN microring is 50 μm. The cross section of the LN microring as indicated by the blue dashed area in Fig. 2(a) is shown in Fig. 2(b). In the current design, the LN microring has a trapezoidal cross-section with a top width of 2.5 μm, a bottom width of 7.5 μm and a height of 800 nm, which is covered by a 1.5-μm-thick SiO_2 cladding layer. The cross section of the coupling area (yellow dashed area in Fig. 2(a)) is shown in Fig. 2(c). The three-layer structure, i.e., LN, SiO_2 and SiN from bottom to top, can be clearly seen. The thickness of the PECVD SiO_2 layer was reduced from 1.5 μm to 600 nm by FIB etching for evanescent light coupling. The rib SiN waveguide was fabricated by FIB etching with a width of 3.5 μm and a rib height of 550 nm.

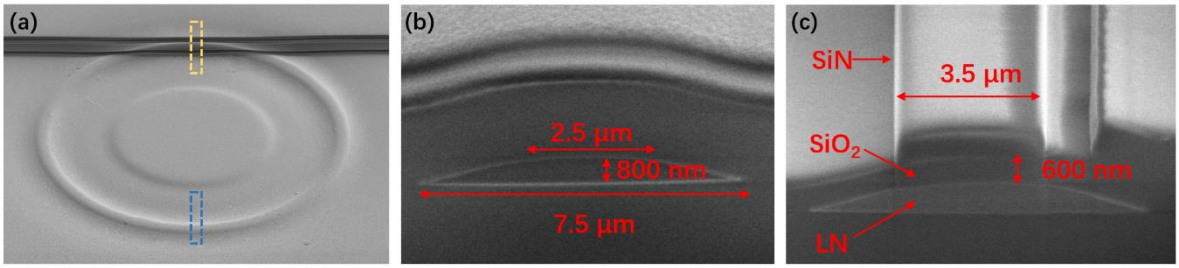

Figure 2. (**a**) Top view SEM image of LN microring resonator and SiN waveguide. (**b**) Sectional view SEM image of the structure at the location of the yellow dashed box in Fig. 2(**a**). (**c**) Sectional view SEM image of the structure at the location of the blue dashed box in Fig. 2(**a**).

To examine the coupling effect of the configuration and characterize the optical mode structure of the LN ring resonator, we used an experimental setup as schematically shown in Fig. 3. A tunable laser (TLB 6728, New Focus Inc., USA) was employed to couple light into and out of SiN waveguide through the with a taper angle of 90°. To enhance the detection signal, the tunable laser was boosted by an erbium-ytterbium-doped fiber amplifier (EYDFA, Golight, Inc.) before coupling into the SiN waveguide. The linewidth of the tunable laser is 200 kHz. The polarization of the pump laser was adjusted by an in-line fiber polarization controller. The Q-factor of resonant mode was measured by

Preprints (www.preprints.org) | NOT PEER-REVIEWED | Posted: 4 November 2020 doi:10.20944/preprints202011.0176.v1

a photodetector (New focus 1811-FC-AC, Newport Inc., USA). We used an arbitrary waveform generator (AFG3052C, Tektronix Inc., USA) to synchronize the tunable laser and oscilloscope signals.

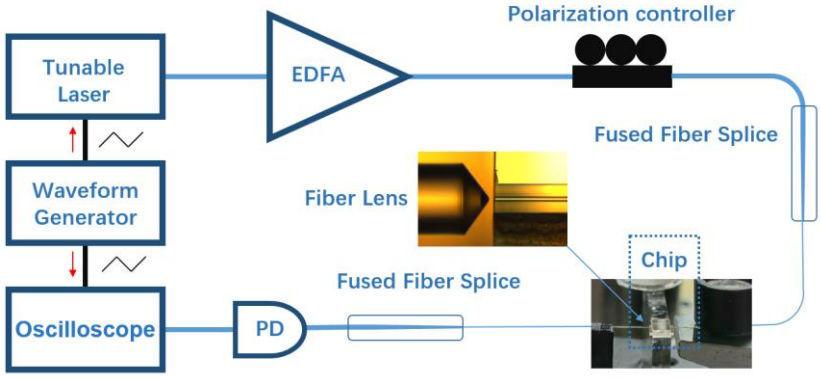

Figure 3. Schematic of experimental testing setup. Inset: optical micrograph of the fiber lens coupling with the SiN waveguide.

Figure 4(a) shows the transmission spectrum for the wavelength range from 1537 nm to 1562 nm. The free spectral range (FSR) of the microresonator was measured to be 3.34 nm. A pair of the splitting whispering-gallery modes at the resonant wavelength around 1543.52 nm was chosen for measurement of the Q-factor by fitting with a Lorentz function. The Q factors were measured to be 1.49×10^7 and 1.09×10^7, respectively, as indicated by the Lorentz curves in Fig. 4(b). The high Q-factor of the LN microresonator indicates that the fabricated device with the vertical integration configuration functions effectively for evanescent light coupling between the LN microring and the SiN waveguide.

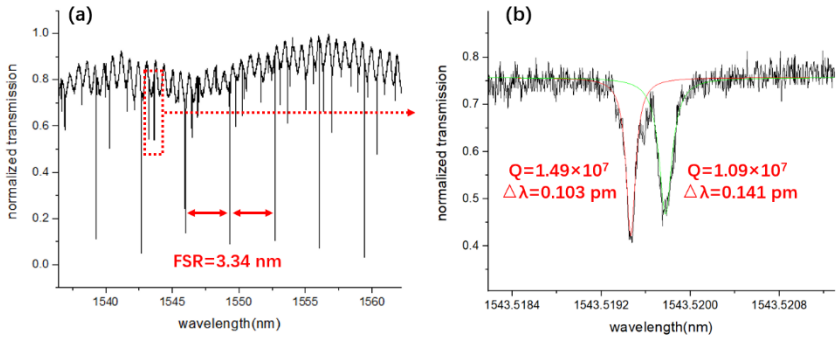

Figure 4. (**a**) Transmission spectrum of the LN microring resonator. (**b**) The Lorentz fitting of the splitting modes at the location of the red dotted box in Fig.4(**a**) reveals a Q-factor of 1.49×10^7 (red solid line) and 1.09×10^7 (green solid line), respectively.

4. Conclusions

To conclude, we have demonstrated efficient evanescent coupling between the crystalline LN microring resonator fabricated by PLACE and the SiN waveguide fabricated by FIB with a vertical configuration. By controlling the distance between the waveguide and microresonator, nearly critical coupling condition has been achieved with ultra-high Q factors, i.e., the Q-factor of the fabricated LN microresonator was measured to be 1.49×10^7. Furthermore, we should point out that the coupling efficiency can be continuously tuned upon demand either by varying the thickness of the SiO_2 cladding layer or changing the relative position between the waveguide and the microring resonator in the horizontal plane. The scheme proposed in this work is also beneficial for large-scale PIC integration as multiple microresonators can be remotely connected on a single chip using the same waveguide and the coupling efficiency can be individually tuned as reasoned above. Thus, the scheme provides a promising photonic integration solution widely adopted by a broad range of LNOI

photonic applications ranging from micro/nano- nonlinear optics and optical interconnect to on-chip artificial intelligence demonstration, etc.

Author Contributions: conceptualization, Y.C.; methodology, Y.C. and W. C.; validation, J.Z., M.W. (Min Wang) and R.W.; formal analysis, J.Z., R.W. W.C. and M.W. (Min Wang); investigation, J.Z., R.W, Z.F. and W.C.; resources, J.Z., M.W.(Miao Wu), M.W.(Min Wang), Z.F., R.W. and J.Z. (Junxia Zhou); data analyze, J.Z., Y.L., W.C. and M.W.(Min Wang); draft preparation, Y.C., W.C and J.Z.; supervision, W.C. and Y.C.; funding acquisition, Y.C. and W.C.

Funding: We acknowledge supports from National Key R&D Program of China (2019YFA0705000), National Natural Science Foundation of China (11674340, 11734009, 11874154, 11874375, 61761136006, 61590934), the Strategic Priority Research Program of CAS (XDB16030300), Shanghai Municipal Science and Technology Major Project (2019SHZDZX01), and Key Research Program of Frontier Sciences, CAS (QYZDJ-SSW-SLH010).

Conflicts of Interest: The authors declare no conflicts of interest.

References

1. Boes, A.; Corcoran, B.; Chang, L.; Bowers, J.; Mitchell, A. Status and potential of lithium niobate on insulator (LNOI) for photonic integrated circuits. *Laser Photon. Rev.* **2018**, 12, 1700256.
2. Diziain, S.; Geiss, R.; Zilk, M.; Schrempel, F.; Kley, E.-B.; Tünnermann, A.; Pertsch, T. Mode analysis of photonic crystal L3 cavities in self-suspended lithium niobate membranes. *Appl. Phys. Lett.* **2013**, 103, 251101.
3. Zhang, M.; Wang, C.; Cheng, R.; Shams-Ansari, A.; Lončar, M. Monolithic ultra-high-Q lithium niobate microring resonator. *Optica*. **2017**, 4, 1536-1537.
4. Hu, H.; Yang, J.; Gui, L.; Sohler, W. Lithium niobate-on-insulator (LNOI): Status and perspectives. *Proc. SPIE.* **2012**, 8431, 84311D.
5. Geiss, R.; Saravi, S.; Sergeyev, A.; Diziain, S.; Setzpfandt, F.; Schrempel, F.; Grange, R.; Kley, E.-B.; Tünnermann, A., Pertsch, T. Fabrication of nanoscale lithium niobate waveguides for second-harmonic generation. *Opt. Lett.* **2015**, 40, 2715-2718.
6. Luo, R.; He, Y.; Liang, H.; Li, M.; Lin, Q. Semi-nonlinear nanophotonic waveguides for highly efficient second-harmonic generation. *Laser Photon. Rev*. **2019**, 13, 1800288.
7. Krasnokutska, I.; Tambasco, J. L. J.; Li, X. J.; Peruzzo, A. Ultra-low loss photonic circuits in lithium niobate on insulator. *Opt. Express*. **2018**, 26, 887-894.
8. Lu, J.; Surya, J. B.; Liu, X.; Xu, Y.; Tang, H. X. Octave-spanning supercontinuum generation in nanoscale lithium niobate waveguides. *Opt. Lett.* **2019**, 44, 1492-1495.
9. He, M.; Xu, M.; Ren, Y.; Jian, J.; Ruan, Z.; Xu, Y.; Gao, S.; Sun, S.; Wen, X.; Zhou, L.; Liu, L.; Guo, C.; Chen, H.; Yu, S.; Liu, L.; Cai, X. High-performance hybrid silicon and lithium niobate Mach–Zehnder modulators for 100 Gbit s^{-1} and beyond. *Nat. Photon*. **2019**, 13, 359-364.
10. Chen, J.-Y.; Ma, Z.-H.; Sua, Y. M.; Li, Z.; Tang, C.; Huang, Y.-P. Ultra-efficient frequency conversion in quasi-phase-matched lithium niobate microrings. *Optica.* **2019**, 6, 1244-1245.
11. Luo, R.; He, Y.; Liang, H.; Li, M.; Lin, Q. Highly tunable efficient second-harmonic generation in a lithium niobate nanophotonic waveguide. *Optica.* **2018**, 5, 1006-1011.
12. Wu, R.; Zhang, J.; Yao, N.; Fang, W.; Qiao, L.; Chai, Z.; Lin, J.; Cheng, Y. Lithium niobate micro-disk resonators of quality factors above 10^7. *Opt. Lett.* **2018**, 43, 4116-4119.
13. Zhang, J.; Fang, Z.; Lin, J.; Zhou, J.; Wang, M.; Wu, R.; Gao, R.; Cheng, Y. Fabrication of crystalline microresonators of high quality factors with a controllable wedge angle on lithium niobate on insulator. *Nanomater.* **2019**, 9, 1218.
14. Wu, R. B.; Wang, M.; Xu, J.; Qi, J.; Chu, W.; Fang, Z. W.; Zhang, J. H.; Zhou, J. X.; Qiao, L. L.; Chai, Z. F.; Lin, J. T.; Cheng, Y. Long low-loss-litium niobate on insulator waveguides with sub-nanometer surface roughness. *Nanomater.* **2018**, 8, 910.
15. Jiang, W. C.; Lin, Q . Chip-scale cavity optomechanics in lithium niobate. *Sci. Rep.* **2016**, 36920
16. Zhang, M.; Buscaino, B.; Wang, C.; Shams-Ansari, A.; Reimer, C.; Zhu, R.; Kahn, J. M.; Lončar, M. Broadband electro-optic frequency comb generation in a lithium niobate microring resonator. *Nature.* **2019**, 568(7752), 373-377.

17. Fang, Z.; Haque, S.; Farajollahi, S.; Luo, H.; Lin, J.; Wu, R.; Zhang, J.; Wang, Z.; Wang, M.; Cheng, Y.; Lu, T. Polygon coherent modes in a weakly perturbed whispering gallery microresonator for efficient second harmonic, optomechanical, and frequency comb generations. *Phys. Rev. Lett.* **2020**,125, 173901.
18. Wang, L.; Wang, C.; Wang, J.; Bo, F.; Zhang, M.; Gong, Q.; Lončar, M.; Xiao, Y.-F. High-Q chaotic lithium niobate microdisk cavity. *Opt. Lett.* **2018,** 43(12), 2917.
19. Wolf, R.; Breunig, I.; Zappe, H.; Buse, K. Scattering-loss reduction of ridge waveguides by sidewall polishing *Opt. Express*. **2018**, 26, 19815–19820.
20. Pant, M.; Towsley, D.; Englund, D.; Guha, S. Percolation thresholds for photonic quantum computing. *Nat. Commun.* **2019,** 10,1070.